ELSEVIER

Physics of the Earth and Planetary Interiors 88 (1995) 1-15

PHYSICS OF THE EARTH AND PLANETARY INTERIORS

From temporal to spatio-temporal chaos (and turbulence?)

Paul Manneville

LADHYX—Laboratoire d'Hydrodynamique, École Polytechnique, 91128 Palaiseau, France
Service de Physique de l'État Condensé, Centre d'Études de Saclay, 91191 Gif-sur-Yvette, France

Received 4 December 1993; revision accepted 28 February 1994

Abstract

In this paper I elaborate on a talk given at the workshop "Physical and numerical modeling of mantle convection and lithospheric dynamics". The main purpose is to present recent advances in the understanding of the transition to turbulence from a theoretical point of view; a more detailed presentation has been given elsewhere. After a brief recall of the chaos picture of turbulence, I discuss the conditions under which it can be acceptable (i.e. when confinement effects control the space dependence of unstable modes), then describe the tools used when the confinement is weak enough to allow for modulations ending in a genuine space–time chaos. A particular scenario called spatio-temporal intermittency is then analyzed. Finally, the connection with hydrodynamic turbulence and the relevance of some of the ideas presented for geodynamics are discussed.

1. Dynamical systems and the 'nature' of turbulence

Turbulence presents itself as a wildly fluctuating flow regime the understanding of which is important for many fields of basic and applied research, as its mixing and transfer properties are strongly enhanced with respect to their molecular counterparts. Following the suggestion of Landau (1944), one can think of turbulence as resulting from a superposition of an infinite number of oscillation modes, the randomness of the regime arising from the absence of knowledge of the initial phase of each mode. However, as stressed originally by Ruelle and Takens (1971), this idea of a mere superposition is in some sense too linear. In fact, nonlinear interactions among a small number of modes generically yield chaotic behavior characterized by a decay of correlations that more appropriately describe a turbulent regime. In this new perspective, the key concept becomes that of strange attractors, i.e. robust objects defined in phase space, attracting trajectories starting from arbitrary initial conditions but characterized by a long-term divergence of trajectories starting from neighboring initial states.

This last property, of utmost importance, is termed sensitivity to initial conditions. It can be illustrated by means of a simple generic example. Let us consider the following iteration:

$$X \mapsto 2X \pmod 1 \tag{1}$$

called the diadic map (Fig. 1(a)) and known to generate chaotic trajectories. A trajectory of this system is the time series X_1, $X_2 \ldots$ issued from some initial condition X_0; it can easily be seen

0031-9201/95/$09.50
SSDI 0031-9201(94)05072-4

that two trajectories initially separated by δX_0 diverge exponentially rapidly with a characteristic (Lyapunov) exponent $\lambda = \log 2$, i.e. $\lim_{\delta X_0 \to 0} |\delta X_n / \delta X_0| \approx \exp \lambda n$ for large n. Representing trajectories as a walk in the complex plane:

$$Z_n = Z_{n-1} + \exp(2\pi i X_n)$$

one can visualize this divergence (Fig. 1(b)) and, further, compare the deterministic but chaotic walk generated by iteration (1) with that given by a truly random walk (Figs. 1(c) and 1(d)).

This comparison is enlightening, as the natural formalism of the Ruelle–Takens theory is that of low-dimensional dynamical systems, i.e. ordinary differential systems with a small number of variables that are functions of time:

$$\frac{\mathrm{d}A_n}{\mathrm{d}t} = F_n(\{A_m; m = 1, \ldots, N\}) \qquad n = 1, \ldots, N \tag{2}$$

Such continuous-time dynamical systems are then quickly reduced to deterministic discrete time systems, i.e. iterations such as (1), using classical tools called Poincaré sections and return maps (for a pictorial introduction, consult the series of volumes by Abraham and Shaw (1983)).

The 'nature' of turbulence as inferred from the Ruelle–Takens theory thus relates to the

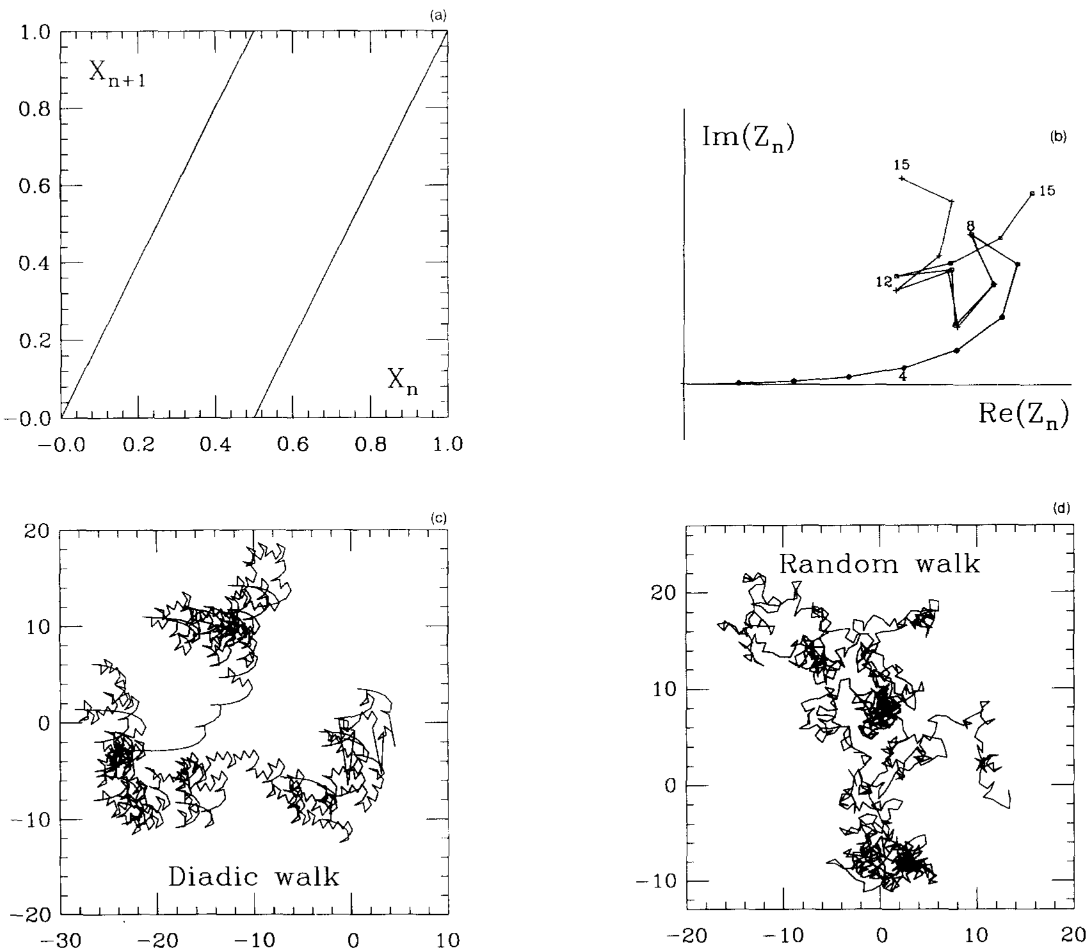

Fig. 1. (a) Diadic map $X \mapsto 2X$ (mod 1). (b) Divergence of neighboring trajectories. (c) Deterministic but chaotic walk. (d) Random walk.

chaotic evolution of the amplitudes $\{A_n\}$ of a small number of well-defined modes. As all the space dependence of the physical system considered is absorbed in the definition of these modes, the term temporal chaos seems most appropriate to describe this picture. Although it is undoubtedly a step forward in understanding how unpredictability enters deterministic systems, the question of its relevance to concrete situations in out-of-equilibrium macroscopic systems still remains to be examined. This is the purpose of the next section.

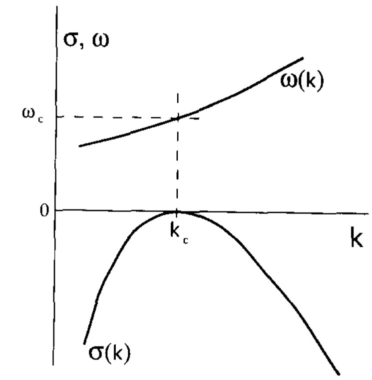

Fig. 2. Generic aspect of real and imaginary parts of the dispersion relation $s = s(k)$ at criticality for an instability producing dissipative waves with wave-vector k_c and pulsation ω_c.

2. Dissipative structures and confinement effects

A question that must certainly be addressed is 'how does the picture emerge?' or, equivalently, 'where do these dynamical systems come from?' To answer this, one has to recall that the modes introduced above are related to physical states induced by instability mechanisms. These states are usually called dissipative structures (Nicolis and Prigogine, 1977); the convection pattern that appears above some critical temperature gradient in a fluid layer heated from below is perhaps the best known and most studied example.

A crucial fact is that the instability mechanism insures a well-defined space–time coherence of spontaneous fluctuations. Schematically, for a periodic pattern in one direction, one can write the field of interest $V(x,t)$ in the form

$$V(x,t) = A\exp(ikx)\exp(st)$$

where A and k are the amplitude and the wave-vector of the fluctuation mode, and $s = \sigma + i\omega$ is the corresponding complex evolution rate. Quantities s and k are related through a dispersion relation $s = s(k;r)$, which is a function of the control parameter r. The real part σ of s tells us whether the given mode grows (is unstable) or decays (is stable) (see Fig. 2).

Different cases are possible according to whether the most unstable mode, i.e. the mode with the largest positive σ, has k_c and/or the corresponding frequency ω_c different from zero. For example, convection in ordinary fluids (plain Rayleigh–Bénard convection) yields a stationary ($\omega_c = 0$) cellular pattern ($k_c \neq 0$) whereas convection in binary mixtures evolves into propagating thermo-diffusive waves ($k_c \neq 0$ and $\omega_c \neq 0$). The case of a uniform oscillatory instability ($k_c = 0$, $\omega_c \neq 0$) can arise in diffusion-reaction systems (Belousov–Zhabotinsky reaction in chemistry).

Fourier modes introduced above are a special case appropriate only for translationally invariant laterally unbounded systems. More generally, one has to use normal modes X_n specific to the geometry of the problem and encoding the characteristic space and time scales of the instability mechanism. These normal modes can be used as a basis for representing arbitrary fluctuations:

$$V = \sum_n A_n X_n$$

each X_n being an eigenvector associated with the eigenvalue $s_n = \sigma_n + i\omega_n$ of the linear stability problem around some basic state. These modes can be ordered by decreasing values of the real part σ_n of their complex growth rate s_n. Strongly stable modes have $\sigma < 0$ with $|\sigma|$ large whereas central, i.e. nearly neutral, modes have $|\sigma|$ small, either negative or positive. Situations of interest for the moment are those where the number n_c of central modes is sufficiently small and the stable modes are sufficiently strongly damped ($|\sigma_n|$ large for $n > n_c$) so that there is a wide gap in the spectrum between the stable and central parts. Then the amplitudes of the stable modes quickly relax toward values imposed by the coupling to unstable modes. They are said to be 'slaved' to the central modes (Haken, 1983). Owing to this property, one can eliminate them 'adiabatically' and obtain an effective system with only the set of central modes coupled together. To illustrate this important process, let us consider a system of only two real modes X_c (amplitude A_c) and X_s (A_s) coupled together through a dynamical system that formally reads

$$\frac{\mathrm{d}A_c}{\mathrm{d}t} = \sigma_c A_c + g_c(A_c, A_s)$$

$$\frac{\mathrm{d}A_s}{\mathrm{d}t} = \sigma_s A_s + g_s(A_c, A_s)$$

and where the relevant assumptions are: (1) σ_c positive or negative but small (mode X_c nearly marginal); (2) σ_s negative and large (mode X_s strongly stable). If the amplitude A_c evolves slowly, as these assumptions imply, then the second equation can be solved for A_s, with A_c considered as a parameter. After a brief transient of duration $\mathscr{O}(1/|\sigma_s|)$, A_s settles to the root of

$$\sigma_s A_s + g_s(A_c, A_s) = 0$$

Schematically, this equation defines a manifold in the space (A_c, A_s). The value found for A_s, denoted as $\tilde{A}_s(A_c)$, is then inserted in the first equation, which becomes

$$\frac{\mathrm{d}A_c}{\mathrm{d}t} = \sigma_c A_c + g_c\left[\left(A_c, \tilde{A}_s(A_c)\right)\right]$$
$$= \sigma_c A_c + g_{\mathrm{eff}}(A_c)$$

i.e. an effective equation for A_c that parametrizes the position of the system on the previously defined manifold. In this case, the degree of freedom A_s has been eliminated and the number of effective degrees of freedom is reduced to one (see Fig. 3).

This possibility of a reduction is important for interpreting the transition to turbulence in continuous media that are infinitely dimensional a priori. Indeed, one can then analyze the bifurcations of the resulting system using tools developed for low-dimensional dynamical systems, write its normal form, and study the corresponding scenarios of transition to temporal chaos, such as period doubling (Feigenbaum, 1983) or intermittency (Pomeau and Manneville, 1980); for a review, readers are referred to Schuster (1988) or Manneville (1990).

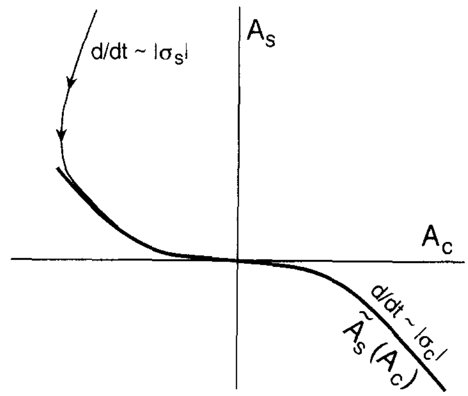

Fig. 3. Reduction to the center manifold: trajectories relax in a time $\mathscr{O}(1/|\sigma_s|)$ toward the manifold $A_s = \tilde{A}_s(A_c)$ and then evolve slowly along it at a rate controlled by σ_c.

Assumptions (1) and (2) above are fulfilled in the presence of strong lateral confinement effects, as the corresponding linear stability problem has a fully discrete spectrum and clearly distinct eigenmodes (e.g. a convection experiment in a cubic box). In this case, one can view the transition to turbulence as a process involving more and more unstable modes via individual bifurcations as the forcing is increased. After a sufficient but small number of bifurcations, chaos is observed to set in. Not too far from the instability threshold, the best representation of the system's evolution remains in terms of a small number of chaotically evolving amplitudes A_n, even though naive observation may suggest strong spatio-temporal fluctuations. Numerous tools have been elaborated to count and identify the relevant modes, e.g. fractal dimension measurements (see Gershenfeld, 1988).

However, when the forcing is further increased, different regimes are entered (soft and hard turbulence in convection; for a review, consult Siggia (1994)). At some stage, the dynamical system approach is no longer appropriate, because too many modes are involved and the representation of the dynamics in a high-dimensional phase space becomes too abstract, i.e. (strictly) temporal chaos ceases to be a good model of turbulence. It may then be legitimate to come back to an approach where physical space has recovered at least part of its natural role.

The above discussion implies that the increase in the number of degrees of freedom is due to a 'filling' of the physical system by structures of smaller and smaller size generated by higher-order instabilities when the control parameter is increased (the revenge of Landau?). In practice, the growth of spatio-temporal chaos is not easily studied in this context where the system lies already far from the primary instability threshold. However, one can immediately realize that there is a case where the number of degrees of freedom can be increased while remaining reasonably close to threshold. This is when the instability mechanism generates a periodic structure with a typical size of the order of some critical wavelength $\lambda_c = 2\pi/k_c$. Indeed, assuming that each cell can be viewed as a unit bearing its own degrees of freedom and the whole system as a lattice of such units coupled to their neighbors, one can suppose that the number of degrees of freedom increases proportionally to the size of the system as measured in terms of its width L relative to λ_c: $\Gamma = L/\lambda_c$ (aspect ratio). Universality and specificities of the routes to turbulence corresponding to this case are the subjects of the next two sections. In practice, we shall be interested in systems where only one physical mode is relevant. Although the emergence of a stationary structure can be accounted for by a single variable, two components merged into a complex variable are needed for an oscillatory mode. We shall then describe the dynamics of the system close to bifurcation by a single equation:

$$\frac{\mathrm{d}A}{\mathrm{d}t} = F_r - \mathcal{N}(A)$$

where the amplitude of the bifurcated state A can be real or complex. Quantity r is the control parameter and $\mathcal{N};(A)$ represents nonlinearities operating beyond the bifurcation point (instability threshold) at $r = r_c = 0$. Solution $A \equiv 0$ is stable below the threshold $r < 0$ and unstable for $r > 0$. The behavior of the bifurcated solution essentially depends on whether the instability becomes saturated or not beyond the threshold, i.e. on the structure of $\mathcal{N};(A)$. In the real case, we shall then consider

$$\mathcal{N};(A) = \epsilon A^3 + A^5 \text{ with } \epsilon = \pm 1 \tag{4}$$

Here, $\epsilon = +1$ corresponds to the supercritical case where the bifurcated solution tends continuously to zero with r as $\sqrt{r}$, i.e. from above (see Fig. 4(a); the fifth-order term is then essentially irrelevant). By contrast, for $\epsilon = -1$, the third-order term is destabilizing, the bifurcation is subcritical. The fifth-order term insures the saturation of the order parameter at a finite value beyond threshold; this discontinuous variation explains that hysteresis cycles can be described by varying the control parameter (see Fig. 4(b)). The

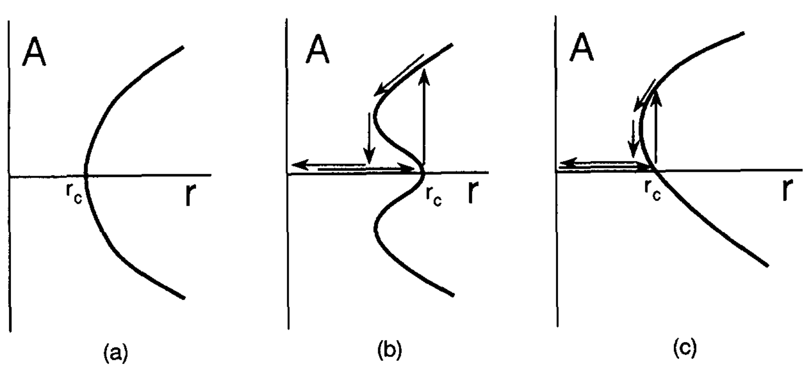

Fig. 4. Typical bifurcation diagrams. (a) Supercritical bifurcation. (b) Subcritical bifurcation. (c) Transcritical bifurcation.

cases described up to now have a built-in $A \to -A$ invariance. The supercritical version is appropriate for plain Rayleigh–Bénard convection under Boussinesq conditions (moderate heating) and symmetrical top and bottom boundaries. When this symmetry is broken or non-Boussinesq effects are taken into account, this invariance property is lost and Eq. (3) must be completed by a lower-order quadratic term A^2, which is able to account for the occurrence of a transcritical bifurcation to a hexagonal pattern (Fig. 4(c)).

In the complex case, coefficients in Eq. (3) above now have an imaginary part (i.e. ϵ replaced by $\epsilon + ic_3$, the coefficient of the fifth-order term being $1 + ic_5$, if necessary). Essentially, the same holds true for the modulus of the order parameter (Hopf bifurcation toward an oscillatory regime, super- or subcritical according to the sign of ϵ).

An important property of the real case is that (3) derives from a potential, known in this context as a Lyapunov function:

$$\frac{\mathrm{d}A}{\mathrm{d}t} = -\frac{\partial G_r}{\partial A}$$

with

$$G_r(A) = -\frac{1}{2}rA^2 + \frac{1}{4}\epsilon A^4 + \frac{1}{6}A^6$$

with the consequence that this quantity decreases monotonically in the course of time:

$$\frac{\mathrm{d}G}{\mathrm{d}t} = \frac{\partial G}{\partial A}\frac{\mathrm{d}A}{\mathrm{d}t} = -\left(\frac{\mathrm{d}A}{\mathrm{d}t}\right)^2 \leqslant 0$$

The extension to the complex case is straightforward as long as coefficients of the evolution equation are real ($G_r = G_r(A, A^*)$ and $\mathrm{d}A/\mathrm{d}t = -\partial G_r/\partial A^*$), but the potential property is lost when the coefficients are complex. The distinction between sub- and supercritical, illustrated in Fig. 4, turns out to be very important when the possibility of modulations appears in weakly confined systems.

3. Envelopes and envelope equations

By contrast with confined systems (aspect ratio of order unity), extended systems are characterized by quasi-continuous linear stability spectra made of branches parametrized by the wave-vector. Neighboring modes thus have comparable structures and only differ by the precise value of their wavelength. Furthermore, a large number of them can be excited close to the threshold. From a linear stability viewpoint, this number grows generically as $\Gamma_{\mathrm{eff}}^{\mathrm{d}}\sqrt{r}$, where Γ is the aspect ratio defined above, d_{eff} is the effective dimensionality of the problem (see Fig. 5) and r, the relative distance to threshold, is assumed to be small enough. In this estimate, the reduction factor $\sqrt{r}$ expresses the fact that each cell does not bring its degrees of freedom independently of its neighbors but has to behave coherently with them. Of course, this reduction effect holds only in the supercritical case when both $r \approx 0$ and $A \approx 0$, because, in the subcritical case, the coherence of the saturated state (A $\approx \mathscr{O}(1)$ even for $r \approx 0$) cannot be estimated without taking nonlinearities into account (see the next section).

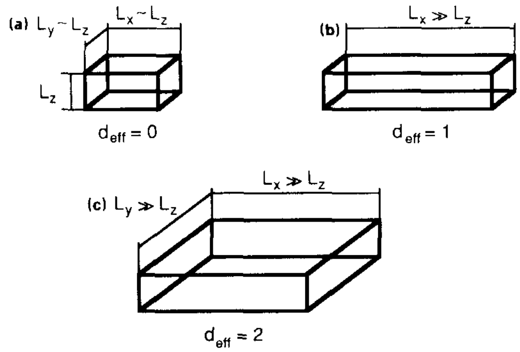

Fig. 5. (a) Confined system with $L_x \approx L_y \approx L_z$. (b) Extended system with effective dimension $d_{\mathrm{eff}} = 1$, $L_x \gg L_y \approx L_z$. (c) Two-dimensional system with $L_x \gg L_z$ and $L_y \gg L_z$.

In fact, in Fourier space, solutions close to threshold can be analyzed as superpositions of modes belonging to the unstable band of width $\sqrt{r}$ around k_c. These solutions are then better understood as modulations superimposed on an ideally periodic pattern with wavelength λ_c. Returning to physical space, one sees that the scale of the allowed modulations varies as $\xi \approx \lambda_c/\sqrt{r}$, that is to say, it diverges at threshold. The coherence length ξ is in fact the right length unit to use for estimating the actual size of the system, i.e. the effective number of degrees of freedom. The interesting parameter range for studying spatio-temporal chaos is then given by the double inequality

$$\lambda_c \ll \xi \ll L$$

The left inequality implies that we remain close to the threshold of the primary instability (which makes analysis possible) and the right one that the system is large; it should be noted that r large means ξ of the order of λ_c, which is helpful for size considerations, but the analysis by perturbation expansions becomes difficult as A is large (as would be also the case for a subcritical bifurcation).

Let us now take nonlinearities into account. For the sake of simplicity, we consider here only the case of a stationary cellular instability ($\omega_c = 0, k_c \neq 0$). We then review the case of a uniform supercritical oscillatory instability ($k_c = 0, \omega_c \neq 0$) which also describes propagating dissipative waves ($\omega_c \neq 0$ and $k_c \neq 0$) in a moving reference frame. More intricate situations occur when the direction of propagation cannot be specified a priori, so that one has to allow for the possibility of standing or traveling waves or, further, when several instability mechanisms are competing.

Beyond the linear stage, one has to describe the effect of nonlinearities on the evolution of the wave packets accounting for the modulated patterns expected close to the threshold. The starting point is the amplitude A of the supposedly uniform ideally periodic pattern at the infinite size limit. Though we deal with a single real mode, we have to modify (3) to take into account translational invariance at the infinite-L limit. For a stationary instability, the solution can be written as

$$V(x,t) = A(t)\cos(k_c x + \phi) + \dots$$

where A is the solution of (3) and the spatial phase variable ϕ specifies the absolute position of the pattern in the laboratory frame. Here the cosine term represents the contribution of the fundamental component at k_c to the complete periodic solution, and the ellipsis suggests the presence of higher-order corrections. In fact, it turns out to be more convenient to understand ϕ as the phase of a complex number still denoted A, i.e. $A = |A|\exp(i\phi)$, so that V now reads

$$V(x,t) = \frac{1}{2}\big[A(t)\exp(ik_c x) + \text{complex conjugate}\big] + \dots$$

For this complex amplitude, Eq. (3) can then be written as (supercritical case)

$$\frac{\mathrm{d}A}{\mathrm{d}t} = rA - |A|^2 A \tag{5}$$

and the solution is easily shown to be indifferent to the value of ϕ ($\mathrm{d}\phi/\mathrm{d}t = 0 \to \phi = \text{constant}$). The important point is that the coefficients in (5) are still real and that the variational property is not lost, as noted above.

In large aspect ratio systems, lateral boundary effects are not able to maintain spatial coherence in the middle of the system. Modulated patterns are therefore expected to be the rule rather than the exception. Though it can be derived more rigorously by means of multi-scale expansions (Newell and Whitehead, 1969), we introduce here the evolution equation for modulations heuristically by assuming that they relax in a diffusive way:

$$\frac{\partial A}{\partial t} = F_r(A) + \nabla^2 A$$

(the diffusivity is normalized to unity by proper rescaling of the lengths).

With F_r as given in (5), one obtains an equation written here in one-dimensional form:

$$\frac{\partial A}{\partial t} = A + \frac{\partial^2 A}{\partial x^2} - |A|^2 A \tag{6}$$

Eq. (6) generically governs the slow space–time modulations of a uniform stationary periodic reference pattern. From the scalar variable A function of time governed by (5), an ordinary differential equation, we we have passed to a field $A(x,t)$ function of time and space governed by (6), a partial differential equation. Slow space dependence means ∇A is small when compared with $k_c A$.

The case of a modulated uniform oscillatory state or that of a propagating wave in a frame moving at its own group velocity can be treated similarly to yield the same equation, but with complex coefficients:

$$\frac{\partial A}{\partial t} = A + (1 + ic_2)\frac{\partial^2 A}{\partial x^2} - (1 + ic_3)|A|^2 A \quad (7)$$

(The need for complex coefficients can be appreciated when taking the limit $(c_2, c_3) \to \infty$ which yields the nonlinear Schrödinger equation, known to account for the dispersion of nearly monochromatic wave trains.)

Eqs. (6) and (7) are generic examples of envelope equations called Ginzburg–Landau equations (GLEs). They are adapted to the description of long-wavelength, low-frequency perturbations to an extended system in the vicinity of its bifurcation point. In fact, the extension to higher effective dimensions may not be as trivial as simply replacing $\partial^2 A/\partial x^2$ by $\nabla^2 A$, because the symmetries of the system have to be taken properly into account (Newell et al., 1993), but this simple extension already offers a rich phenomenology of space–time behavior.

Modulations can have basically two origins. The most obvious one is extrinsic, i.e. imposed by the presence of lateral boundaries at large but finite distance; for example, $A(x = \pm L/2) = 0$. The other one is intrinsic, either because the uniform solution is unstable or because field A can support topological defects. A spectacular example of the latter is the spiral solution of the two-dimensional complex GLE, which corresponds to a zero of $|A|$ accommodating a rotation of $\pm 2\pi$ of the phase around it (see Fig. 6).

The next step in the study of the transition to spatio-temporal chaos is to examine the stability of special solutions of Ginzburg–Landau-like equations. The main difference between the real and complex cases come from the 'potential' structure of the equation with real coefficients. In the real case (stationary instability), the equation derives from a potential. Accordingly, the asymptotic time behavior is a monotonic relaxation toward some static configuration (any non-trivial asymptotic time dependence can derive only from higher-order non-variational contributions neglected at this stage). This does not mean that the final solution is simple, because it has to accommodate the boundary conditions. For example, in the two-dimensional case, straight rolls have a tendency to be perpendicular to the boundary; however, this condition cannot be fulfilled in a

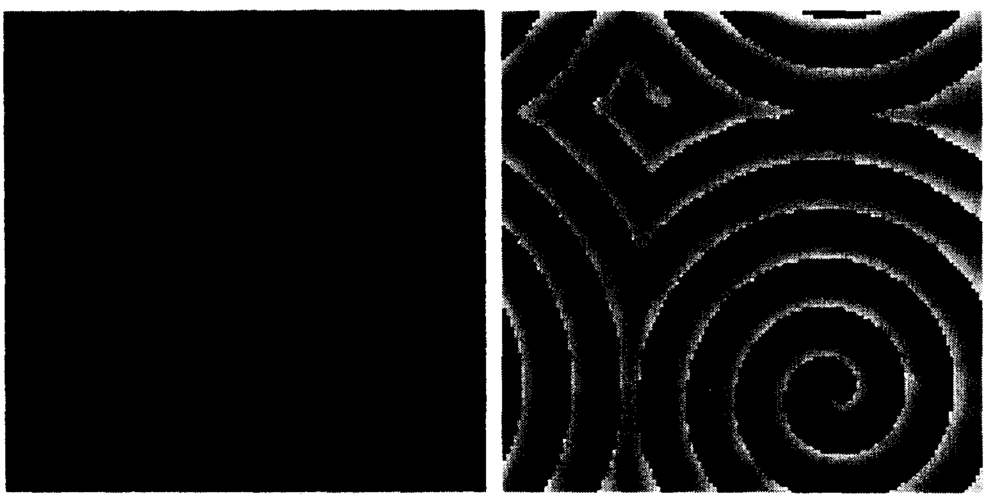

Fig. 6. Gray-level image of the modulus and phase of a solution $A(x,y,t)$ of the two-dimensional complex GLE for $c_2 = -2.0$ and $c_3 = 0.8$ with periodic boundary conditions at $L = 128$. Left: modulus, $|A| = 0$ is black, $|A| = |A|_{max}$ is white. Right: phase represented by equally spaced gray levels over a 2π interval. Here the system has frozen on a spiral state; owing to the boundary conditions, the waves emitted by the spiral collide to form steady shocks at the intersection of which one finds another zero of the amplitude.

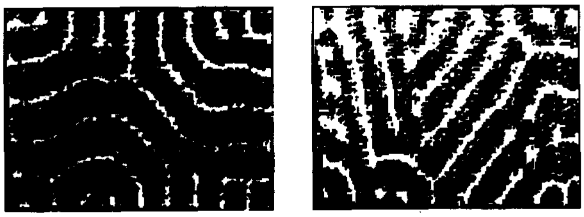

Fig. 7. Two examples of patterns observed in high Prandtl number convection (reproduced with permission of P. Bergé and M. Dubois).

closed container without introducing some curvature or grain boundaries linking domains with different orientations or other defects such as dislocations. As a result, disordered textures are usually obtained. These textures attempt to minimize the frustration generated by the presence of lateral boundaries, and this adjustment can take a very long time in large systems. Indeed, we have to deal with a diffusive behavior on a scale $\mathscr{O}(L)$ that takes at least a time $\mathscr{O}(L^2)$. This framework is well adapted to the description of textured patterns observed in high Prandtl number convection, such as those illustrated in Fig. 7. In low Prandtl number fluids, non-variational contributions come into play early on, possibly generating weak turbulence in the form of time-dependent disordered patterns. In the oscillatory case, the variational structure is lost from the beginning and the time dependence is expected to be much more active already for the one-dimensional case (see below).

Intrinsic modulations can also be generated by secondary instabilities. In this context, dangerous modes are often related to the translation invariance of the problem at the infinite-L limit. Indeed, among possible perturbations, those corresponding to a local translation of the solution can be viewed as slight modifications of the global translation mode. This mode is neutral in the absence of boundary effects, and one can easily imagine that such perturbations could be slightly unstable. Local translations are directly interpreted in terms of the phase variable ϕ introduced above, which, uniform and time-independent in the basic state, becomes modulated as the result of specific instability modes. As an example, let us consider a long-wavelength compression mode corresponding to a phase that varies sinusoidally in the direction of the wave-vector of a system of stationary rolls. When the wave-vector k_0 of the underlying pattern differs sufficiently from the critical value, this mode becomes

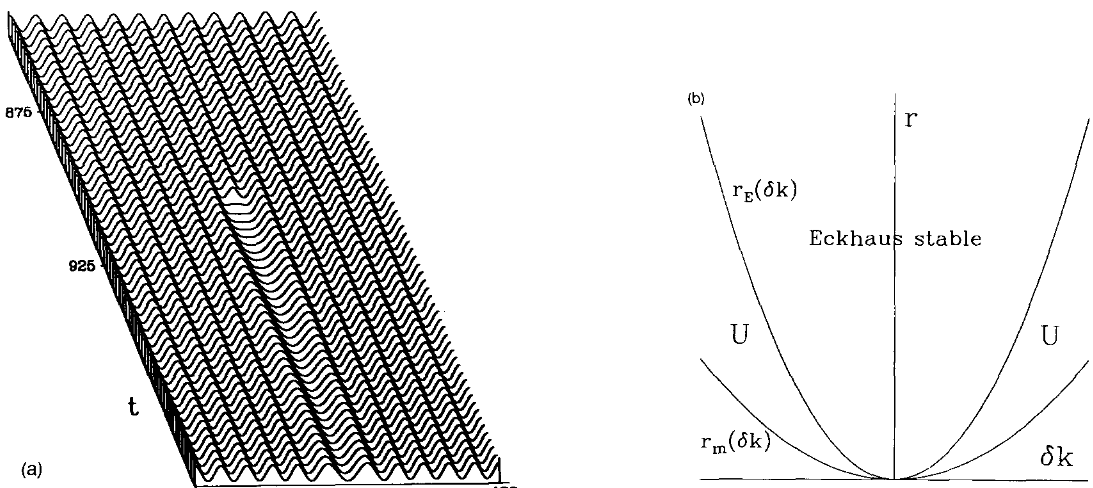

Fig. 8. (a) Illustration of the collapse of a pair of rolls induced by a slight local compression of a pattern whose wave-vector k lies in the Eckhaus-unstable domain (regions 'U' in (b) between the marginal stability curve $r_m(k) = (1 - \delta k^2)^{1/2}$ and the Eckhaus threshold $r_E(k) = (1 - 3\delta k^2)^{1/2}$, where $\delta k = k_0 - k_c$).

unstable (Eckhaus instability): the phase modulation increases up to the birth or collapse of a pair of rolls (Fig. 8(a)). This instability is universal in the sense that its threshold does not depend on the mechanism that induces the dissipative structure but only on the distance to the critical point: $r_E = [(k_0 - k_c)/3]^{1/2}$. At given k_0, the pattern is Eckhaus-unstable for $r < r_E$} (Fig. 8(b)).

As already pointed out, the case of the complex GLE is expected to yield much more 'turbulent' situations. The plan of parameters (c_2,c_3) as defined by (7) has been studied thoroughly, and different regimes of space–time chaos have been identified (for a review of results in the one-dimensional case, see Chaté (1995)). The main distinction between these regimes may be the presence of amplitude defects, i.e. points in space where the phase ϕ of the complex field A cannot be defined because the modulus $|A|$ vanishes. The starting point here is the study of the stability of plane wave solutions to (7) with wave-vector k_0:

$$A(x,t) = A_0\exp[i(k_0x - \omega_0 t)]$$

with $|A_0|^2 = 1 - k_0^2$ and $\omega_0 = c_3 + (c_2 - c_3)k_0^2$. These solutions exist for $k_0^2 < 1$, but they can be unstable with respect to side-band modes of Eckhaus type. When $1 + c_2c_3 < 0$ (Newell's criterion) all solutions are unstable, even the uniform one ($k_0 = 0$); this is the so-called Benjamin–Feir instability (BF for short). As before, the phase of the solution is a slow variable, and one can expect parameter sets for which the modulus of the solution is slaved to the phase. When this is the case, the gradient of the phase, $\psi = \partial_x\phi$, which measures the local wave-vector of the phase modulation ϕ, can be shown to be governed at lowest order by the Kuramoto–Sivashinsky equation (KSE) (Kuramoto and Tsuzuki, 1976; Sivashinsky, 1977):

$$\partial_t\psi + \psi\partial_x\psi = -\partial_{xx}\psi - \partial_{xxxx}\psi$$

In this equation, the anti-diffusive term $-\partial_{xx}\psi$ derives directly, by rescaling, from a diffusion coefficient varying as $(1 + c_2c_3)$ which becomes negative in the BF-unstable range. The interest of the KSE lies in the fact that it spontaneously displays turbulent solutions when the length of the system is large enough. Furthermore, this so-called phase turbulence regime turns out to be extensive, in the sense that the amount of chaos is proportional to the length of the system (see Manneville, 1988).

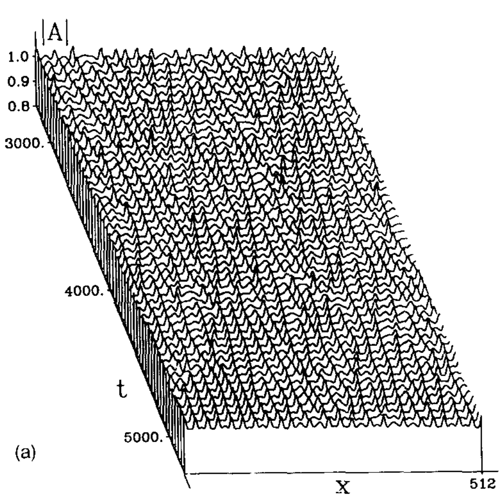

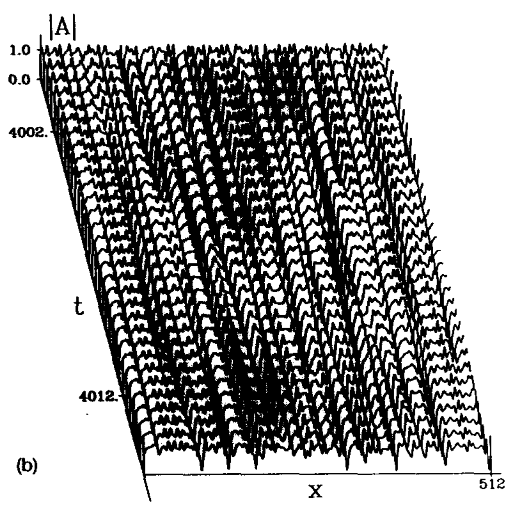

Fig. 9. Space–time evolution of $|A|$ for the 1D-CGLE. (a) Phase-turbulence regime for $c_2 = -2.0$, $c_3 = 0.7$, $1 + c_2c_3 = -0.4$. (b) Amplitude–turbulence regime for $c_2 = -2.0$, $c_3 = 1.25$, $1 + c_2c_3 = -1.5$; periodic boundary conditions at $L = 512$. (Note the variation range of $|A|$ in each case.)

For the one-dimensional complex GLE (1D-CGLE), there is some numerical evidence from simulations that phase turbulence —understood as a regime where $|A|$ is bounded away from zero so that the phase ϕ is defined everywhere (see Fig. 9(a))—exists closely enough to the BF-line (see the discussion by Chaté (1995)). This seems (experimentally) true when the linear dispersion (c_2 term) is comparatively large; however, when the non-linear contribution becomes important, i.e. $1/c_3$ is comparatively small, this may not be the case: the phase gradient can diverge locally, which allows the vanishing of $|A|$. The 1D-CGLE can then enter a regime of amplitude turbulence where $|A|$ varies wildly (Fig. 9(b)). In this case, space–time chaos can be understood from the viewpoint of the dynamics of a population of 'defects'. Present knowledge on the different regimes observed in the 1D-CGLE is summarized in Fig. 10. The study of the two-dimensional case is in progress (amplitude and phase regimes and the stability of spirals).

Studying model equations of the same kind as the GLEs reviewed above is of considerable help in understanding the transition to spatio-temporal chaos in realistic cases such as Rayleigh–Bénard convection, as they offer a framework that is far more simple than primitive hydrodynamic equations (e.g. Boussinesq) and yet is sufficient to deal with universal features of pattern formation.

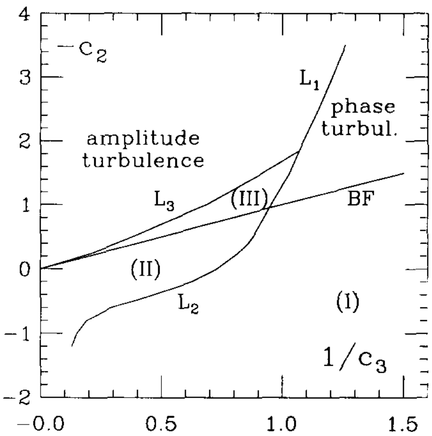

Fig. 10. Diagram displaying the different regimes observed in simulations of the 1D-CGLE as a function of $1/c_3$ and $-c_2$ (adapted from Chaté, 1995) BF: Benjamin–Feir instability line given by $1+c_2c_3=0$; plane waves are linearly stable below this line. In region (II), above line L_2, they are metastable against a spatio-temporally intermittent regime involving localized 'defect solutions' whereas in region (I), below this line, they attract all initial conditions except some solitary waves stable close to line L_2. In region (III), between line BF, line L_3 and line L_2, amplitude turbulence and phase turbulence coexist ('bi-chaos'). Line L_1 marks the smooth transition from amplitude turbulence to phase turbulence (the density of amplitude defects goes to zero when approaching line L_1 from the left).

4. Spatio-temporal intermittency

Up to now, we have considered systems in which the transition to chaos is rather progressive: supercritical primary instability saturating gently beyond threshold and spatio-temporal chaos understood in terms of envelope modes. However, as already noted by Landau (1944), a much wilder situation can take place when there is no stable bifurcated state in the neighborhood of the state that loses stability. In the case of low-dimensional systems (i.e. that of strong confinement) this fundamentally subcritical case leads generically to attractor coexistence in state space, to bifurcations displaying characteristic hysteretic features, or to crises (Grebogi et al., 1983). In extended systems, this coexistence of attractors in state space translates into a coexistence in physical space of different regimes, each in its own domain and separated from the others by a discontinuity region called a front.

As stressed by Pomeau (1986), an original route to turbulence, called spatio-temporal intermittency (STI), can take place when two states are in competition, one being regular and the other chaotic but metastable, i.e. having a finite lifetime. In this case, the transition then presents itself generically as a contamination process, the locally chaotic state occupying turbulent patches, spots, puffs, slugs, etc., and the regular state corresponding to the part of the system which is still laminar. When the control parameter is increased, one can observe the transition from a fully laminar state to a fully turbulent regime by

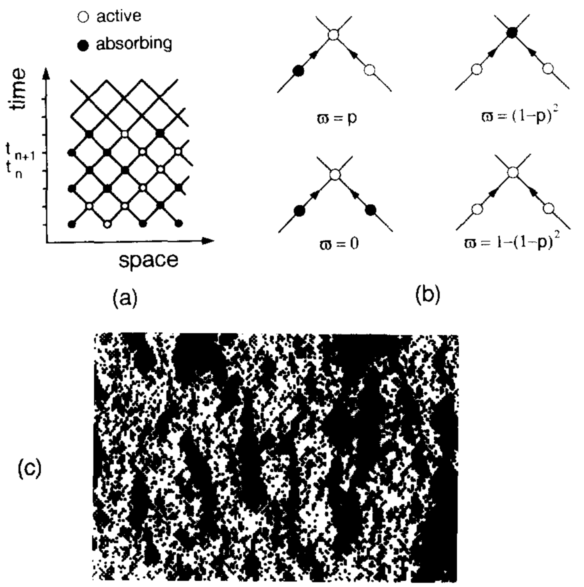

Fig. 11. Directed percolation on a one-dimensional lattice. (a) Sites can be in active (white) or absorbing (black) states. (b) Probability of the different configurations as a function of the contamination probability p. (c) Evolution of a randomly initialized lattice for $p \approx p_c$.

monitoring the turbulent fraction, i.e. either the fraction of space occupied by the turbulent state or the fraction of time the system remains in the chaotic state at a given place. The transition can be continuous in the sense that the turbulent fraction increases continuously from zero, whereas the local state of the system can change discontinuously in physical space.

The existence of two well-distinguished states strongly suggests the use of binary coding 'laminar/turbulent', 'dead/alive', 'up/down', 'black/white', etc. By assuming that chaos present at some sites can contaminate neighboring laminar states with some probability p, one arrives at a model akin to directed percolation. This fully stochastic process is a mathematical idealization applicable, e.g. to the flow of a liquid through a porous medium: whether the fluid can percolate through it or remain trapped in it depends on the void fraction that is interpreted as the local probability of having a given channel between grains open or not. The problem is then to find the probability that a given site inside the medium is 'wet' or 'dry', or else to find continuous directed paths of open channels. Other current applications pertain to forest fires or epidemics. In the present context, this process is used to characterize a specific turbulent regime where chaotic domains coexist with regular domains, as described above.

When studied in the framework of statistical physics, directed percolation is a process defined on a lattice with two possible states per site. The probability for one site at time $t+1$ to be in a given state is a function of the transition probability p and the configuration of its neighborhood on time t. One of the states has to be absorbing, i.e. it cannot become active by itself but only through contamination from active neighbors at a previous time (see Fig. 11). When the contamination probability is small, the 'epidemic' stops, but beyond a well-defined threshold p_c, it does not stop. In the context of flow through porous media, this simply means that a given channel cannot be wet if all its parent channels are dry and that when the void fraction is sufficiently large the fluid can percolate to infinity ('directed' meaning essentially one-way; for a review, consult Kinzel (1983)). Beyond a threshold, the contaminated fraction is observed to vary as a power law: $F = (p - p_c)^{\beta}$, where β is a 'critical exponent' in the terminology of phase transitions. This exponent is believed to take some universal value depending only on the dimensionality of the lattice on which the process is defined.

Specially designed deterministic models of such a contamination process have been built with units that are governed by a local dynamics allowing for transient chaos toward a steady state. An example is given in Fig. 12: local maps $X^{t+1} = f(X^t)$ such as that described in Fig. 12(a) are sitting in a row (one-dimensional model) and coupled to nearest neighbors in a diffusive way (Chaté and Manneville, 1991):

$$X_j^{t+1} = f(X_j^t) + \epsilon\left[f(X_{j+1}^t) - 2f(X_j^t) + f(X_{j-1}^t)\right]$$

Local transient chaos is present in each map for $X < 1$ (owing to a slope r larger than two, active state); the regular (laminar, absorbing) state corresponds to the domain $X > 1$. The transition is observed upon varying the diffusion constant ϵ. The coupling, provided it is strong enough, is able to convert local transient temporal chaos into sustained spatio-temporal chaos (see Fig. 12(b)). For this particular case, the turbulent fraction is seen to increase as $F \approx (\epsilon - \epsilon_c)^\beta$ with $\beta \approx 0.25$; the value expected from directed percolation using the universality assumption would be $\beta = 0.28$. Owing to limitations inherent in numerical simulations (limited amount of data), it is not easy to decide whether a given transition to turbulence via STI is in the same universality class as directed percolation, but models such as that introduced in Fig. 12(a) clearly show that, being sensitive to the nature of the local dynamics, the process is clearly not universal. Indeed, the transition can be continuous or discontinuous and, when it is continuous, the critical exponents depends up on local features (controlling, e.g. the existence of propagating, soliton-like, structures visible in Fig. 12(b)).

This transition can be observed in models such as the 1D-CGLE, but also in laboratory experiments, for example, convection in a narrow annular gap at moderate to high Prandtl numbers (Ciliberto and Bigazzi, 1988; Daviaud et al., 1989) or 'printer instability' (Rabaud et al., 1990). The understanding gained by its study can also help us better describe other transitions involving turbulent spots, e.g. in plane Couette flow or in the Blasius boundary layer flow.

5. Further problems

In this paper, it has been attempted to summarize recent progress in understanding the emergence of spatio-temporal chaos, with emphasis on the role of physical confinement by lateral boundary effects. Apparently, this restricts the approach to the case of flows taking place in a closed container, e.g. natural convection, and excludes open flows, i.e. flows where the fluid goes through the set-up, tube, channel, etc. In the latter case, new features can appear as a consequence of the average transport of matter. These new features relate to the absolute or convective nature of the instability (see, Huerre, 1987). Schematically, when the effect of downstream advection dominates the instability mechanism, one can observe the growth of the unstable modes

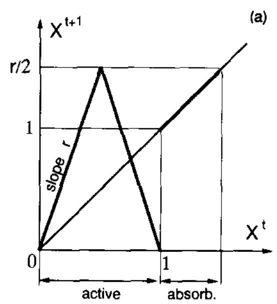

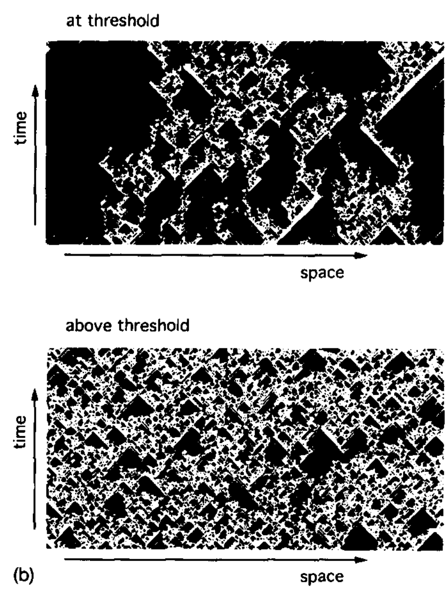

Fig. 12. Transition to turbulence via STI. (a) Local map. (b) Regimes observed for $\epsilon \approx \epsilon_c$ (top), and $\epsilon \gg \epsilon_c$ (bottom). Active sites ($X < 1$) are black and sites in the absorbing state ($X > 1$) white.

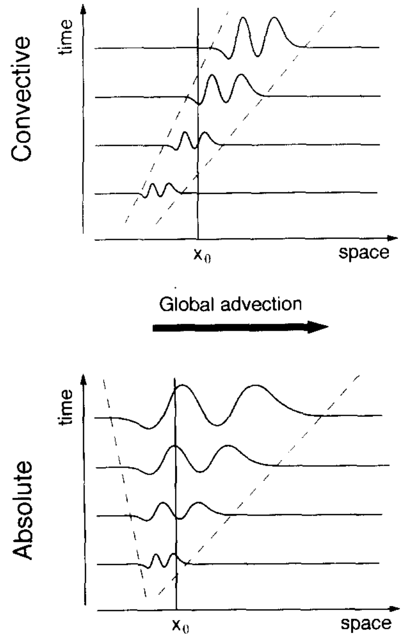

Fig. 13. Absolute and convective instabilities in an open flow system.

only in a frame moving at the average speed of the flow, not in the laboratory frame; if the residence time of the fluid in the set-up is insufficient, the instability is not observed. In this case, the instability is called convective. When, on the contrary, the mechanism is stronger than the advection effect, the instability is observed in the laboratory frame in spite of the downstream transport. Such an instability is said to be absolute (see Fig. 13).

In practice, the situation may be not so clear-cut, owing to the development of the flow downstream. Indeed, the global advection kept constant in space, the local strength of the mechanism can vary with the distance to some special point in the flow. For example, in the wake of an obstacle, the instability can be absolute just behind the obstacle and convective further downstream. The domain of absolute instability is roughly limited to the region of recirculation, which presents itself as a hydrodynamic resonator with properties akin to those of a confined system, though there is no physical confinement along the flow direction (see Oertel, 1990). On another hand, the absolute–convective distinction can become relevant even in closed systems, when the instability involves dissipative waves that have to accommodate end effects, as, for example, for convection in binary mixtures (Cross, 1986). The recourse to simplified models in terms of envelopes, i.e. variants of the Ginzburg–Landau equations introduced above, is a prerequisite to the study of the concrete situations found in hydrodynamics.

Further steps are still necessary before an understanding of developed turbulence is obtained, in particular with respect to the emergence of scaling in the so-called inertial range, where the energy cascades from large scales where it is injected by instability mechanisms to small scales where it is dissipated by viscous damping. It seems possible to understand this hierarchy of scales as resulting from the successive excitation of modes in the spirit of Landau. In fact, the stress has recently been put on large-scale coherent structures on the one hand and on the generation of filaments in fully developed turbulence on the other (Tabeling, 1995). In turbulent convection at high Rayleigh numbers, boundary-layer instability at low to moderate Prandtl numbers or plume generation and motion at higher Pr have received much attention (Siggia, 1994).

The account given may suggest that the advances thus far are mainly conceptual; nevertheless, one can hope to apply some of these findings to concrete situations of geophysical fluid—not forgetting, of course, all the specificities of the problem considered (e.g. convection), its geometry (e.g. a spherical shell), the nature of the fluid (i.e. its Prandtl number), etc. Use can certainly be made of the methods developed (modeling by envelope equations, coupled maps) and the vast catalog of behaviors already discovered in pattern dynamics (amplitude and phase turbulence, defect stability, spatio-temporal intermittency, etc.). Also, analog reasoning stemming from the study of 'universal' features of spatio-temporal chaos can be of great help in clearly distinguishing what is relevant to temporal chaos, spatio-temporal chaos, or turbulence, and in choosing the best tools to attack the geophysical phenomenology.

References

Abraham, R.H. and Shaw, D.C., 1983. Dynamics: the Geometry of Behavior. Aerial Press, Santa Cruz, USA.

Campbell, D. and Rose, H. (Editors), 1983. Order in Chaos. North Holland, Amsterdam (reprint of Physica D, Vol. 7).

Chaté, H., 1995. In: Spatiotemporal Patterns in Nonequilibrium Complex Systems. Santa Fe Institute Series in the Sciences of Complexity. Addison Wesley, New York, in press.

Chaté, H. and Manneville, P., 1991. In: P. Coullet and P. Huerre (Editors), New Trends in Nonlinear Dynamics and Pattern-forming Phenomena. Plenum, New York.

Ciliberto, S. and Bigazzi, P., 1988. Spatio-temporal intermittency in Rayleigh–Bénard convection. Phys. Rev. Lett., 60: 286.

Cross, M.C., 1986. Traveling and standing waves in binary convection. Phys. Rev. Lett., 57: 2935.

Daviaud, F., Bergé, P. and Dubois, M., 1989. Europhys. Lett., 9: 441.

Feigenbaum, M.J., 1983. In: D. Campbell and H. Rose (Editors), Order in Chaos. North Holland, Amsterdam (reprint of Physica D, Vol. 7).

Gershenfeld, N., 1988. An experimentalist's introduction to the observation of dynamical systems. In: B.-L. Hao (Editor), Directions in Chaos, Vol. 2. World Scientific, Singapore.

Grebogi, C., Ott, E. and Yorke, J.A., 1983. In: D. Campbell and H. Rose (Editors), Order in Chaos. North Holland, Amsterdam (reprint of Physica D, Vol. 7).

Haken, H., 1983. Synergetics. Springer, Heidelberg.

Huerre, P., 1987. In: E. Tirapegui and D. Villaroel (Editors), Instabilities and Nonequilibrium Structures. D. Reidel, Dordrecht.

Kinzel, W., 1983. Directed percolation. In: G. Deutscher, R. Zallen and J. Adler (Editors), Percolation Structures and Processes. Ann. Isr. Phys. Soc., Vol. 5.

Kuramoto, Y. and Tsuzuki, T., 1976. Persistent propagation of concentration waves in dissipative media far from thermal equilibrium. Prog. Theor. Phys., 55: 356.

Landau, L.D., 1944. On the nature of turbulence. Dokl. Akad. Nauk SSSR, 44: 339. English translation in: D. ter Haar (Editor): Collected Papers of L.D. Landau. Pergamon, Oxford, pp. 387–391.

Manneville, P., 1988. The Kuramoto–Sivashinsky equation: a progress report. In: Wesfreid et al. (Editors), Propagation in Far-from-equilibrium Systems. Springer Series in Synergetics, Vol. 41. Springer, Heidelberg.

Manneville, P., 1990. Dissipative Structures and Weak Turbulence. Academic Press, Boston, MA.

Newell, A.C. and Whitehead, J., 1969. Finite bandwidth, finite amplitude convection. J. Fluid Mech., 38: 279.

Newell, A.C., Passot, T. and Lega, J., 1993. Order parameter equations for patterns. Annu. Rev. Fluid Mech., 25: 399.

Nicolis, G. and Prigogine, I., 1977. Self-organization in Nonequilibrium Systems, from Dissipative Structures to Order through Fluctuations. Wiley, New York.

Oertel, Jr., H., 1990. Wakes behind blunt bodies. Annu. Rev. Fluid Mech., 22: 539.

Pomeau, Y., 1986. In: A.R. Bishop, G. Grüner and B. Nicolaenko (Editors), Spatio-temporal Coherence and Chaos in Physical Systems. North Holland, Amsterdam (reprint of Physica, D, Vol. 23).

Pomeau, Y. and Manneville, P., 1980. Intermittent transition to turbulence in dissipative dynamical systems. Commun. Math. Phys., 74: 189.

Rabaud, M., Couder, Y. and Michalland, S., 1990. Dynamical regimes of directional viscous fingering: spatiotemporal chaos and wave propagation. Phys. Rev. Lett., 64: 184.

Ruelle, D. and Takens, F., 1971. On the nature of turbulence. Commun. Math. Phys., 20: 167; addendum, 23: 344.

Schuster, H.G., 1988. Deterministic Chaos. Physics Verlag, Weinheim.

Siggia, E.D., 1994. High Rayleigh number convection. Annu. Rev. Fluid Mech., 26: 137.

Sivashinsky, G.I., 1977. Nonlinear analysis of hydrodynamic instability in laminar flames. Part 1: derivation of basic equations. Acta Astronaut., 4: 1177.

Tabeling, P. (Editor), 1995. A Tentative Dictionary of Turbulence. Plenum, New York.